Available online at www.sciencedirect.com
SCIENCE DIRECT®
Scripta Materialia xxx (2006) xxx–xxx
Scripta MATERIALIA
www.actamat-journals.com

Thermal stability of Al–Cr–N hard coatings

H. Willmann [a,b,*], P.H. Mayrhofer [c,d], P.O.Å. Persson [b,e], A.E. Reiter [f], L. Hultman [b,d], C. Mitterer [c,g]

[a] Materials Center Leoben, Franz-Josef Strasse 13, 8700 Leoben, Austria
[b] IFM Material Physics, Division of Thin Film Physics, Linköping University, 58183 Linköping, Sweden
[c] Department of Physical Metallurgy and Materials Testing, University of Leoben, 8700 Leoben, Austria
[d] Materials Chemistry, RWTH-Aachen, 52074 Aachen, Germany
[e] FEI Company, 5651 GG Eindhoven, The Netherlands
[f] Balzers Ltd., 9496 Balzers, Liechtenstein, Germany
[g] Christian Doppler Laboratory for Advanced Hard Coatings, University of Leoben, 8700 Leoben, Austria

Received 1 December 2005; received in revised form 9 February 2006; accepted 14 February 2006

Abstract

Heat treatment of arc-evaporated cubic $Al_{0.7}Cr_{0.3}N$ hard coatings in Ar up to 1450 °C causes precipitation of AlN. The Cr-enriched matrix transforms into Cr via Cr_2N under N_2 release. These reactions are investigated by simultaneous thermal analysis, mass spectrometry, X-ray diffraction, and analytical transmission electron microscopy.

Keywords: Differential scanning calorimetry; Thermogravimetric analysis; Analytical electron microscopy; Decomposition; AlCrN

1. Introduction

Hard protective coatings are widely used to expand the usability of cutting and metal forming tools. Important requirements are sufficient hardness, high wear-, corrosion-, and oxidation-resistance as well as good thermal stability. In modern cutting applications such as high-speed and/or dry cutting, the temperature at the cutting edge can exceed 1000 °C [1,2]. Consequently, the applied protective coating must be capable of withstanding these extreme conditions. $Al_xCr_{1-x}N$ provides high hardness [3–12], superior oxidation-resistance [11–15], and good tribological behavior [9–11,16]. These properties depend on chemical composition and microstructure [8,9,14,17] and when optimized, excellent performance in cutting tests can be obtained [17]. While the oxidation-resistance is discussed intensively in the literature [11–15,17], the temperature dependent structural and compositional evolution is essentially unexplored. Two stability-related questions are discussed in the literature. The first addresses the limit of Al solubility in the face-centered cubic (fcc) CrN phase [9,17–20], while the second deals with the onset of decomposition of the supersaturated phase into its stable constituents [13,14,16,17].

Several deposition techniques and setups are reported for synthesizing $Al_xCr_{1-x}N$ coatings [6,9,11,12,17,19]. Recent results conclude that there are improved mechanical and thermal properties with an increased Al content in the fcc-structure (up to $x = 0.75$) [12–14,17]. Exceeding the solubility limit for Al results in a hexagonal wurtzite type (w) structure [17,19,20] and the mechanical properties degrade [12,17]. Consequently, $Al_{0.7}Cr_{0.3}N$ coatings, which have been shown to have an excellent performance in cutting tests [17], are the focus of this work.

* Corresponding author. Address: Materials Center Leoben, Franz-Josef Strasse 13, 8700 Leoben, Austria. Tel.: +43 38424024237; fax: +43 38424024202.
E-mail address: herbert.willmann@unileoben.ac.at (H. Willmann).

1359-6462/$ - see front matter © 2006 Published by Elsevier Ltd. on behalf of Acta Materialia Inc.
doi:10.1016/j.scriptamat.2006.02.023

Here, we used a combination of differential scanning calorimetry (DSC), thermal gravimetric analysis (TGA) and mass spectrometry (MS), to investigate the decomposition process of supersaturated cubic $Al_{0.7}Cr_{0.3}N$ coatings in detail. X-ray diffraction (XRD) and scanning transmission electron microscopy (STEM) in combination with energy dispersive X-ray analysis (EDX) were utilized to attribute the observed DSC, TGA, and MS results. The complex decomposition process of supersaturated $Al_{0.7}Cr_{0.3}N$ coatings is described.

2. Experimental details

The depositions were carried out using a Balzers Rapid Coating System, described in Ref. [17]. The equipment was operated in the cathodic arc evaporation setup with four metallic compound targets (Al/Cr at.% ratio = 70/30). The target current was 140 A, the base pressure was below 1×10^{-3} Pa, and the nitrogen pressure during the reactive deposition process was 3.5 Pa. A bias voltage of −40 V was applied to the substrates and their temperature was kept at 500 °C. Twofold substrate rotation [17] was used to obtain uniform film properties. The substrates were cleaned by plasma etching prior to deposition.

A Netzsch STA 409C instrument with a quadrupole mass spectrometer (QMS) connected through a skimmer coupling system was used for DSC, TGA, and MS measurements as well as for annealing samples for subsequent XRD and TEM investigations. To avoid the influence of the substrate material in the DSC measurements, the coatings were chemically removed from their low-alloyed steel substrates using a 10 mol% nitric acid. After filtering and cleaning, the film material was mechanically ground to a fine powder whereof ~30 mg was used for each measurement. Dynamic heating up to 1450 °C was performed in a flow of Ar (50 sccm, 99.999% purity) using a heating rate of 20 K/min. The DSC system was calibrated for temperature and sensitivity by the pure elements Sn, Zn, Al, Ag, and Au. To detect N_2, the atomic mass unit 28 was monitored by the QMS.

XRD measurements of as-deposited and annealed samples were carried out on a Siemens D500 diffractometer in the Bragg-Brentano (θ–2θ) geometry using Cu Kα radiation.

The electron microscopy investigations were obtained from plan-view samples deposited on single crystal sapphire discs (Al_2O_3, ∅3 mm × 0.1 mm, (0 0 0 1) oriented). Due to the high annealing temperatures (T_a), sapphire was chosen to avoid interdiffusion of substrate and film material. STEM was performed on a Tecnai G^2 TF 20 UT microscope operating at 200 keV. The probe size used was <1 nm and the images were recorded with a high-angle annular dark field (HAADF) detector. A camera length of 90 mm was used to promote preferential mass-thickness contrast and to reduce the influence of diffraction contrast. Chemical compositions were measured with energy dispersive X-ray analysis (EDX) during STEM investigations.

3. Results and discussion

EDX measurements showed that the chemical composition of the as-deposited coatings was $Al_{0.7}Cr_{0.3}N$, corresponding to the Al/Cr ratio in the target.

Fig. 1(a) shows a typical DSC signal and the mass loss for $Al_{0.7}Cr_{0.3}N$ as a function of the annealing temperature. The monitored N_2 signal of the MS measurement is presented in Fig. 1(b). This signal starts to deviate from the baseline at $T_a \sim 925$ °C, where the onset of sample mass loss can also be detected in TGA. During the heat treatment up to 1450 °C, several reactions in the film material are superimposed, which is indicated by the overlapping reaction peaks in the DSC and MS signal as well as by the changing slopes of the TGA curve. As the release of nitrogen is directly connected to mass loss, any change in the MS signal corresponds to a change in TGA and vice versa. Both measurement techniques indicate an incomplete decomposition process even at 1450 °C, i.e., the MS signal does not reach the baseline, and the TGA signal is not horizontal.

Various exothermic and endothermic reactions can correspondingly be detected by DSC up to 1450 °C (Fig. 1(a)). The first exothermic reaction with a peak maximum at ~625 °C (onset slightly higher than the deposition temperature), is related to recovery processes [21–23]. Deposition-induced lattice defects, responsible for a compressive residual stress state, anneal out due to increased diffusivity at elevated temperatures.

XRD investigations were performed on samples annealed at temperatures indicated in Fig. 1(a) in order to explain the reactions detected via DSC, TGA, and MS. Fig. 2(a) shows diffractograms of these specimens

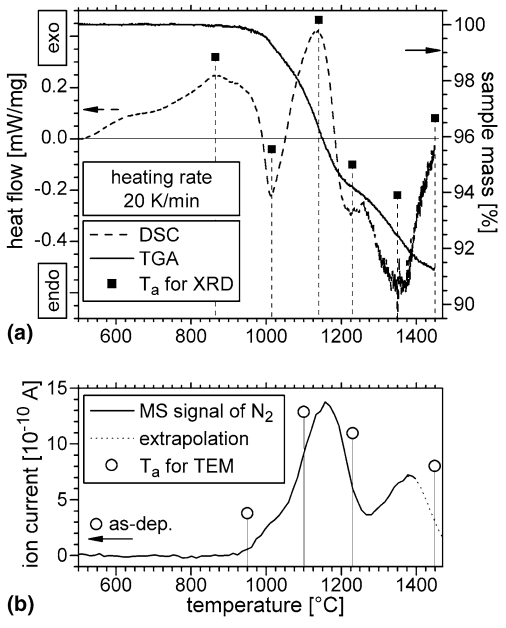

Fig. 1. (a) DSC and TGA of $Al_{0.7}Cr_{0.3}N$ in inert atmosphere with indicated annealing temperatures for XRD measurements; (b) corresponding MS signal with marked temperatures for TEM investigations.

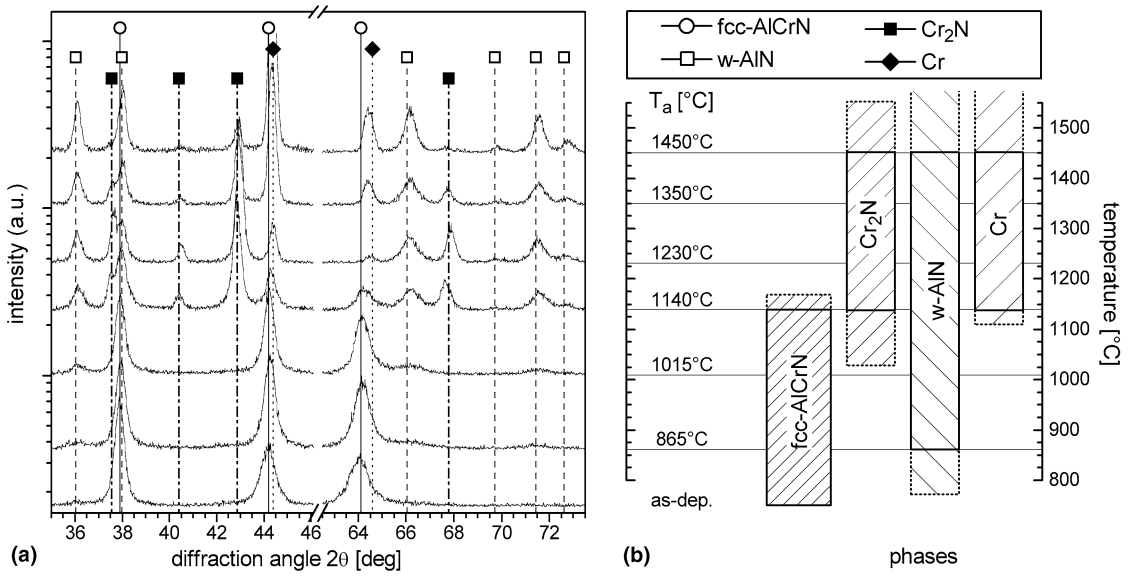

Fig. 2. (a) XRD evolution of an $Al_{0.7}Cr_{0.3}N$ film with annealing temperature; (b) bars represent detected phases, dashed extensions indicate the estimated existence range of the phases that occur.

including positions for fcc-AlCrN, located between fcc-CrN and fcc-AlN, as well as w-AlN, hexagonal (hex) Cr_2N, and body-centered cubic (bcc) Cr. The lattice parameter for Cr_2N is between the values given by different JCPDS-files [24]. For the sample annealed at 865 °C the (200) and (220) AlCrN matrix peaks show a reduced full width at half maximum of ~23% confirming the above mentioned recovery effects during annealing. The thermal stability range of the phases present during decomposition of $Al_{0.7}Cr_{0.3}N$ is schematically summarized in Fig. 2(b).

For detailed investigation of the as-deposited structure, selected area electron diffraction (SAED) was performed on a plan-view sample. Fig. 3(a) shows the STEM image obtained with minor variations in contrast resulting from different orientated grains. The HAADF image contrast mechanism in this work is optimized for changes in mass and thickness and these parameters are almost uniform for this sample. The uniform contrast indicates a negligible contribution due to diffraction effects for the experimental conditions used. The corresponding SAED pattern is presented in Fig. 3(b). In addition to the diffraction rings from the fcc-structured polycrystalline AlCrN matrix, weak w-AlN reflexes can be detected (Fig. 3(b)). This is not confirmed by XRD results (Fig. 2(a)), which show no w-AlN in the as-deposited state. It has been reported [25] that different substrate materials can influence the structure of AlCrN formed during deposition. However, the grazing incidence XRD of the coating on sapphire shows a diffractogram comparable to the one shown in Fig. 2(a), i.e., also without w-AlN reflexes. SAED of a coating on a cemented carbide substrate shows a pure cubic structure. We therefore conclude that small amounts of w-AlN phase (below the detection limit of XRD) are present in the as-deposited coatings on sapphire.

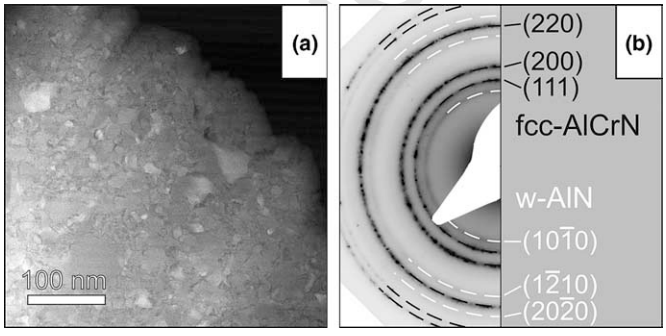

Fig. 3. (a) STEM plan-view image (HAADF) of $Al_{0.7}Cr_{0.3}N$ in the as-deposited state; grains appear in a uniform grey tone, a thickness induced contrast-gradient is superposed; (b) SAED pattern with standard diffraction rings for fcc-AlCrN and w-AlN.

For $T_a = 865$ °C, small fractions of w-AlN can be detected even by XRD, and with higher T_a their peak intensity increases continuously (Fig. 2(a)). The corresponding nucleation and growth processes result in an exothermic contribution to the DSC signal, represented by a broad peak with a detected maximum at ~875 °C (Fig. 1(a)). It is reasonable to estimate the real peak temperature at temperatures above 900 °C since a strong endothermic contribution related to decomposition is superimposed at $T_a > 925$ °C. Simultaneously, the XRD patterns show a reduction in the AlCrN matrix peak intensity for increasing T_a (Fig. 2(a)). The decrease is small for 865 °C < T_a < 1015 °C, becomes pronounced for higher temperatures and for $T_a \geqslant 1230$ °C fcc-AlCrN is below the detection limit. The formation of AlN precipitates leads to a gradual Cr enrichment of the matrix. After obtaining a sufficient driving force from a combination of temperature and chemical composition of the matrix, the release of nitrogen is initiated (see the MS signal in Fig. 1(b)) and consequently the sample mass decreases (Fig. 1(a)). This

decomposition of the material results in an endothermic reaction during DSC measurement with a maximum slightly above 1000 °C.

The reduction of N-content in the matrix also causes a transformation into hex-Cr_2N. For the ideal case, without any remaining Al in the matrix, it is proposed that the stoichiometry of fcc-CrN approaches $CrN_{0.5}$ before transforming into hex-Cr_2N. A corresponding phase transformation causes an exothermic contribution to the DSC measurement of $Al_{0.7}Cr_{0.3}N$, which is now depleted in N. Furthermore the slope of the TGA signal also changes, indicating a different N-release rate compared to the cubic structure. During XRD investigations Cr_2N can be detected in samples annealed between 1140 and 1450 °C. At atmospheric pressure, depending on ambient atmosphere, bulk Cr_2N starts to decompose into bcc-Cr and N_2 gas at temperatures below 1000 °C [26]. This predicted decomposition can first be seen in our material at 1140 °C. The decomposition is visible during DSC as a pronounced endothermic reaction (see Fig. 1(a), reaction peak maximum at ~1350 °C) and the reduced mass-loss slope in the TGA signal. Additionally, an exothermic contribution to the DSC scan results from the transformation from hex into bcc lattice. In the temperature range 1000–1450 °C several endothermic and exothermic reactions are superimposed, and hence the separation of individual contributions to the DSC signal is difficult. Fig. 1(b) indicates the N-release of the Cr_2N decomposition by the MS peak maximum at ~1380 °C. The maximum intensity of Cr_2N during XRD investigations is obtained for samples annealed at 1230 °C. The bcc-Cr phase can be observed for $T_a \geqslant 1140$ °C as a shoulder of the matrix peak at $2\theta \sim 64.6°$. After annealing the films at 1450 °C, mainly w-AlN and bcc-Cr with small fractions of hex-Cr_2N (Fig. 2(a)) are present. The latter explains the uncompleted N-release for $T_a = 1450$ °C as detected by TGA. This is also proven by MS measurements. Because of the high thermal stability of AlN (~2800 °C), we propose that the reduction in sample mass is due to the loss of chromium-bonded nitrogen. Our results indicate that this loss is completed at ~1550 °C for the annealing conditions used (see Fig. 2(b)).

To further verify the obtained results of DSC, TGA, MS, and XRD, the microstructural changes of the material were investigated by TEM for samples annealed at 950, 1100, 1230, and 1450 °C (indicated in Fig. 1(b)). The obtained STEM images are presented in Fig. 4(a)–(d), respectively. Assuming only a minor change in thickness across the investigated sample area, the image contrast may be attributed to pure mass (density) changes, where low atomic mass appears dark.

The sample annealed at 950 °C (Fig. 4(a)) shows precipitates (dark regions), next to coarsened matrix grains, along triple junctions and at grain boundaries. Chemical analysis by EDX confirms that these are composed of Al and N. The surrounding areas of these AlN precipitates are consequently Cr-enriched and appear bright in Fig. 4(a). The bright tissue is generated from sites of early decomposition,

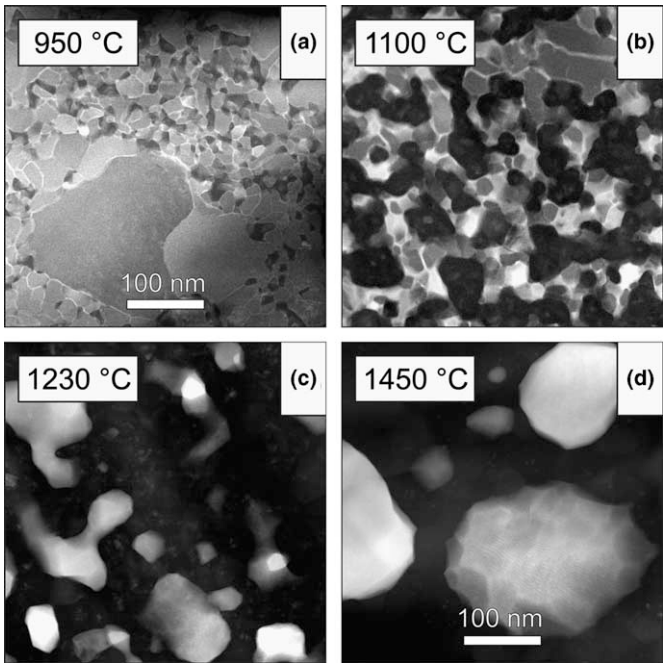

Fig. 4. STEM plan-view images (HAADF) of $Al_{0.7}Cr_{0.3}N$ after annealing at (a) 950 °C; (b) 1100 °C; (c) 1230 °C; (d) 1450 °C.

most probably from grain and phase boundaries. This also corresponds well with the MS measurement, where a small N-release (maximum at $T_a \sim 1015$ °C) slightly before the main peak (maximum at $T_a \sim 1140$ °C) suggests that this phase separation process starts with weakly bonded nitrogen leaving from the grain and phase boundaries.

The sample annealed at 1100 °C (Fig. 4(b)) shows an increase in the volume fraction of AlN precipitates. The bright tissue is more pronounced and the Cr-enriched areas, which form next to these precipitates, can be verified by EDX to have the chemical composition of Cr_2N. This is in agreement with XRD where Cr_2N is detected for samples annealed at $T_a \geqslant 1140$ °C.

Increasing the annealing temperature to 1230 °C (Fig. 4(c)) generates a microstructure where w-AlN grains almost completely encapsulate the initial matrix grains. Growth and increase in the volume fraction of these AlN precipitates is the main reason for the more pronounced w-AlN XRD peaks (see Fig. 2(a)). EDX analysis confirms the described decomposition process of the matrix into Cr via Cr_2N. The intermediate stage of this reaction at 1230 °C can be seen in Fig. 4(c), where Cr and Cr_2N appear with different contrasts.

In Fig. 4(d) ($T_a = 1450$ °C) spherically shaped grains up to 0.5 μm in size embedded in AlN are visible. The coarsening is driven by the potential for the system to reduce its total interfacial energy which is measured as heat release in the DSC. The presence of Cr_2N grains at this temperature, as indicated by XRD, could be confirmed by TEM/EDX investigations. An EDX line scan across the grains displayed in Fig. 4(d) is shown in Fig. 5, including the distribution of the elements Al, Cr, and N and their fits. The

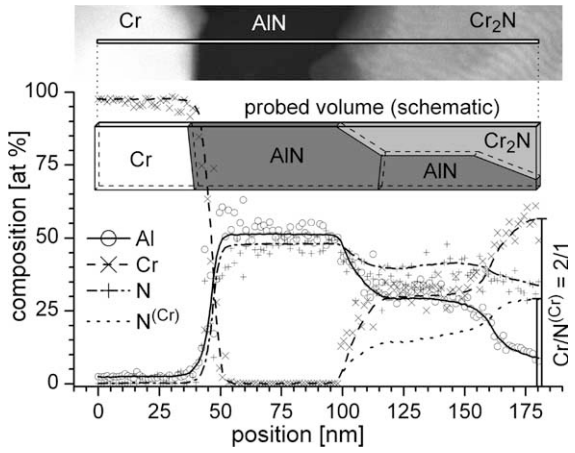

Fig. 5. EDX line scan at an $Al_{0.7}Cr_{0.3}N$ sample annealed at 1450 °C. Fitted curves for Al, Cr, and N are provided. $N^{(Cr)}$ shows N bonded to Cr. The schematic drawing indicates the probed volume under the line scan.

signal labeled $N^{(Cr)}$ represents the nitrogen bonded to Cr under the assumption of stoichiometric AlN presence. The resulting ratio of Cr to $N^{(Cr)}$ equals 2:1, which corresponds to a chemical composition of Cr_2N. The measurement indicates an overlap of two AlN and Cr_2N grains. A schematic illustration of the probed volume is included in Fig. 5.

4. Conclusions

The arc-evaporated $Al_{0.7}Cr_{0.3}N$ hard coatings under investigation are supersaturated fcc-structured in the as-deposited state. During annealing in an inert atmosphere up to 1450 °C at 20 K/min the material undergoes decomposition with several superimposed reactions. After recovery which occurs at temperatures slightly above the deposition temperature, formation and growth of w-AlN precipitates at grain boundaries and triple junctions can be seen, and hence the matrix becomes Cr-enriched. Further annealing causes N-loss (for $T_a > 925$ °C) and subsequently transformation to Cr via the intermediate step of Cr_2N, which is completed at 1550 °C under the used conditions. Fcc-structured AlCrN matrix can be detected during annealing up to 1140 °C, which indicates a stabilization of the Cr–N bonds by Al. At 1450 °C the structure is mainly composed of bcc-Cr and w-AlN with minor fractions of hex-Cr_2N left.

Our results clearly demonstrate the potential of AlCrN coatings for ageing processes with precipitations, which offer explanations for the superior mechanical properties of this material even at high temperatures.

Acknowledgements

The authors want to thank Dr. Jörg Neidhardt (Christian Doppler Laboratory for Advanced Hard Coatings at the University of Leoben) for the support in sample deposition. We are also grateful to Jens Emmerlich (IFM – Thin Film Physics, Linköping University) for the support in the grazing incidence XRD measurement. H.W. is grateful for the Marie Curie fellowship for supporting his stay in Linköping. P.H.M. is supported by the Erwin Schrödinger Program (Project J2469-N02) of the Austrian Science Fund. L.H. acknowledges support from the Swedish Research Council (VR). The work done in Leoben was supported by the Technologie Impulse G.m.b.H within the framework of the K-plus competence center program and by the Christian Doppler Society.

References

[1] Nomura T, Moriguchi H, Tsuda K, Isobe K, Ikegaya A, Moriyama K. Int J Refract Met Hard Mater 1999;17:397.
[2] Modern metal cutting. Sweden: Tofters Tryckeri AB; 1994. p. I-32.
[3] Wuhrer R, Yeung WY. Scripta Mater 2004;50:1461.
[4] Knotek O, Atzor M, Barimani A, Jungblut F. Surf Coat Technol 1990;42:21.
[5] Kawate M, Kimura A, Suzuki T. J Vac Sci Technol A 2002;20(2):569.
[6] Ulrich S, Holleck H, Ye J, Leiste H, Loos R, Stüber M, et al. Thin Solid Films 2003;437:164.
[7] Lugscheider E, Bobzin K, Hornig T, Maes M. Thin Solid Films 2002;420–421:318.
[8] Hasegawa H, Suzuki T. Surf Coat Technol 2004;188–189:234.
[9] Ide Y, Nakamura T, Kishitake K. In: Second international conference on processing materials for properties. San Francisco, CA. Warrendale (PA): The Minerals, Metals and Materials Society; 2000. p. 291.
[10] Okumiya M, Griepentrog M. Surf Coat Technol 1999;112:123.
[11] Vetter J, Lugscheider E, Guerreiro SS. Surf Coat Technol 1998;98:1233.
[12] Hirai M, Ueno Y, Suzuki T, Jiang W, Grigoriu C, Yatsui K. Jpn J Appl Phys 2001;40:1056.
[13] Kawate M, Hashimoto AK, Suzuki T. Surf Coat Technol 2003;165:163.
[14] Banakh O, Schmid PE, Sanjinés R, Lévy F. Surf Coat Technol 2003;163–164:57.
[15] Smith RJ, Tripp C, Knospe A, Ramana CV, Kayani A, Gorokhovsky V, et al. J Mater Eng Perform 2004;13(3):295.
[16] Lugscheider E, Bobzin K, Bärwulf S, Hornig T. Surf Coat Technol 2000;133–134:540.
[17] Reiter AE, Derflinger VH, Hanselmann B, Bachmann T, Sartory B. Surf Coat Technol 2005;200:2114.
[18] Kimura A, Kawate M, Hasegawa H, Suzuki T. Surf Coat Technol 2003;169–170:367.
[19] Makino Y, Nogi K. Surf Coat Technol 1998;98:1008.
[20] Sugishima A, Kajioka H, Makino Y. Surf Coat Technol 1997;97:590.
[21] Mayrhofer PH, Hörling A, Karlsson L, Sjölén J, Larsson T, Mitterer C, et al. Appl Phys Lett 2003;83:2049.
[22] Mayrhofer PH, Clemens H, Mitterer C. Z Metallkd 2005;5:468.
[23] Mayrhofer PH, Mitterer C, Hultman L, Clemens H. Prog Mater Sci [accepted].
[24] Powder Diffraction File (Card 11-0065 for fcc-CrN, Card 46-1200 for fcc-AlN, Card 25-1133 for w-AlN, Card 35-0803 and 3-1191 for hex-Cr_2N, Card 06-0694 for bcc-Cr). International Center for Diffraction Data, JCPDF – ICDD; 1998.
[25] Sun Y, Wang H, Seow HP. J Mater Sci 2004;39:7369.
[26] Gmelins Handbuch der anorganischen Chemie. Weinheim: Verlag Chemie; 1962. p. 160.